JOURNAL OF PETROLOGY | VOLUME 00 | NUMBER 0 | PAGES 1–15 | 2009 | doi:10.1093/petrology/egp007
Journal of Petrology Advance Access published February 27, 2009

Crystal Size Distribution of Periclase in Contact Metamorphic Dolomite Marbles from the Southern Adamello Massif, Italy

T. MÜLLER[1]*, L. P. BAUMGARTNER[1], C. T. FOSTER, JR[2] AND J. R. BOWMAN[3]

[1]INSTITUT DE MINERALOGIE ET GEOCHIMIE, UNIVERSITE DE LAUSANNE, BATIMENT L'ANTHROPOLE, CH-1015 LAUSANNE, SWITZERLAND

[2]DEPARTMENT OF GEOLOGY, UNIVERSITY OF IOWA, IOWA CITY, IA 52242, USA

[3]DEPARTMENT OF GEOLOGY AND GEOPHYSICS, UNIVERSITY OF UTAH, SALT LAKE CITY, UT 84112, USA

RECEIVED SEPTEMBER 10, 2007; ACCEPTED JANUARY 21, 2009

Crystal size distributions (CSD) of periclase in contact metamorphic dolomite marbles are presented for two profiles near the Cima Uzza summit in the southern Adamello Massif (Italy). The database was combined with geochemical and petrological information to deduce the controls on the periclase-forming reaction. The contact metamorphic dolomite marbles are exposed at the contact of mafic intrusive rocks and are partially surrounded by them. Brucite is retrograde and pseudomorphs spherical periclase crystals. Prograde periclase growth is the consequence of limited infiltration of water-rich fluid at T *near 605°C. Stable isotope data show depletion in* ^{13}C *and* ^{18}O *over a narrow region (~40 cm) near the magmatic contact, whereas the periclase-forming reaction front extends up to 4 m from the contact. CSD analyses along the two profiles show that the median grain size of the periclase crystals does not change, but that there is a progressively greater distribution of grain sizes, including a greater proportion of larger grains, with increasing distance from the contact. A qualitative model, based on the textural and geochemical data, attributes these variations in grain size to changing reaction affinities along a kinetically dispersed infiltration front. This study highlights the need to invoke disequilibrium processes for metamorphic mineral growth and expands the use of CSDs to systems of mineral formation driven by fluid infiltration.*

KEY WORDS: *X-ray* μ*C-tomography; contact metamorphism; fluid infiltration; crystal size distribution; 3D; stable isotopes; Adamello Massif*

INTRODUCTION

Metamorphic rock textures are the result of neo-formation of minerals. The spatial distribution of minerals, their shape and size result from the interaction of nucleation, growth, reaction, and deformation. They reflect the rates of change in physicochemical conditions, such as pressure (P), temperature (T), and fluid composition. During the last two decades the focus of metamorphic petrology has changed from a static point of view (i.e. the representation of a mineral assemblage as a single point in a petrogenetic grid) towards a dynamic view that interprets chemical zoning within minerals (e.g. garnet) in terms of time-paths of changing P–T conditions (Spear, 1993). Today much focus is on the dynamic non-equilibrium processes that govern the formation of mineral textures (Carlson & Denison, 1992; Carlson *et al.*, 1995; Lasaga, 1998; Carlson & Gordon, 2004; Hirsch & Carlson, 2006) and mineral zoning as a result of disequilibrium processes in an attempt to decipher the crystallization history (Albarède & Bottinga, 1972; Watson & Liang, 1995; Watson, 1996; Skora *et al.*, 2006). Theoretical calculations based on experimentally derived reaction rate data (e.g. Lasaga & Rye, 1993) as well as textural studies (Roselle *et al.*, 1997; Müller *et al.*, 2004) provide clear evidence for significant disequilibrium during crystal growth. It is increasingly clear that reaction kinetics have a strong influence on the formation of metamorphic minerals, hence understanding these kinetic

*Corresponding author. Present address: Institut für Geologie, Mineralogie und Geophysik, Ruhr-Universität Bochum, D-44780 Bochum, Germany. Telephone: +49-234-322 4141.
E-mail: Thomas.H.Mueller@rub.de

processes is one of the keys to decipher the detailed reaction history of a rock reflected by its metamorphic textures.

Information about the crystallization history is recorded not only in the chemical zoning of minerals but also in the size distribution of the crystals. Crystal size distributions (CSD) provide essential information about the interaction between nucleation and growth of minerals. Crystal size studies in metamorphic rocks have led to models for nucleation and growth processes (Galwey & Jones, 1963, 1966; Kretz, 1966, 1969, 1993; Cashman & Ferry, 1988; Carlson & Denison, 1992; Carlson *et al.*, 1995, 1999). CSDs have been introduced into the Earth Sciences for both magmatic and metamorphic systems (Cashman & Ferry, 1988; Cashman & Marsh, 1988; Marsh, 1998). Subsequent studies focused on regional and contact metamorphic systems where minerals formed as a result of changes in T or P (Kretz, 1966, 1993; Carlson & Denison, 1992; Carlson *et al.*, 1995, 1999, Hirsch *et al.*, 2003; Moazzen & Modjarrad, 2005; Hirsch & Carlson, 2006). However, to the authors' knowledge there is no study describing CSDs of metamorphic minerals that have grown as a result of fluid infiltration.

Several previous studies have described contact metamorphic periclase marbles from the southern Adamello Massif, Italy (e.g. Callegari, 1962; Bucher-Nurminen, 1982; Gerdes *et al.*, 1999). Mineral formation in these marbles is the result of fluid infiltration (Gerdes *et al.*, 1999). This study combines measured CSDs of brucite marbles with geochemical data to evaluate the reaction kinetics of periclase formation.

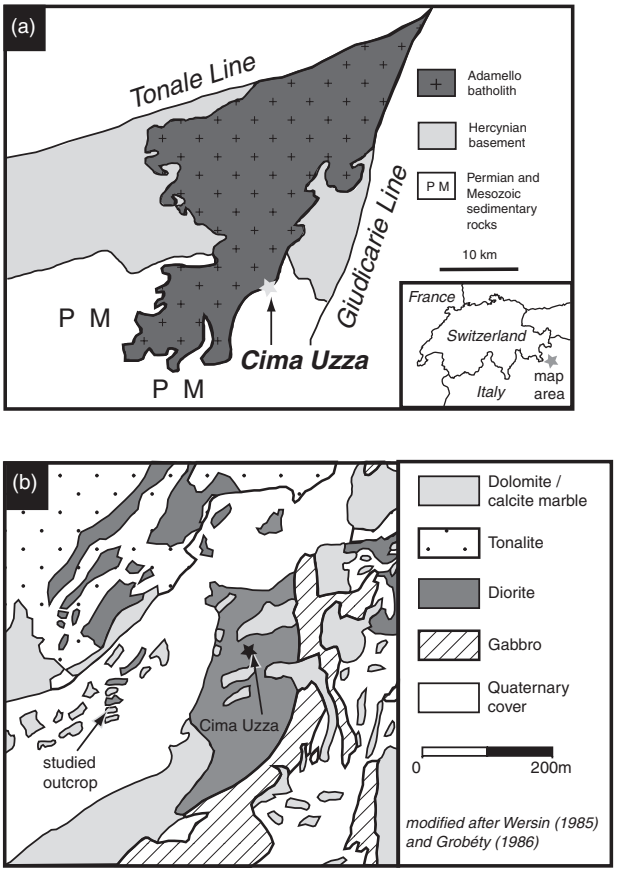

Fig. 1. (a) Generalized map of the Adamello region (Italy), modified after Gerdes *et al.* (1995). Periclase skarns studied are from the Cima Uzza area located at the southern margin of the Adamello batholith. (b) Geological map of the Cima Uzza area (Adamello Massif, Italy) modified after Wersin (1985) and Grobéty (1986).

GEOLOGICAL SETTING

The Adamello Massif is one of the major Tertiary igneous complexes in the Alpine chain. The massif is bordered by the Insubric lineament, the Tonale Line segment to its north and the Giudicarie Line system to the SE (Fig. 1a). The batholith represents a complex series of intrusions, is dominated by rocks of tonalitic to granodioritic compositions, and is accompanied by numerous small bodies of gabbroic and dioritic rocks (Callegari & Dal Piaz, 1973; Bucher-Nurminen, 1982; von Blanckenburg *et al.*, 1998; Colombo & Tunesi, 1999; Pennacchioni *et al.*, 2006). The batholith intruded into Hercynian crystalline basement and Permian to Mesozoic sedimentary rocks of the Southern Alps.

The Cima Uzza area, located at the SE margin of the batholith, exposes Triassic dolomites with minor silicate phases in contact with intrusive igneous rocks (Callegari, 1962). The contact metamorphism of these siliceous dolomites has been the subject of several studies (Callegari, 1962; Bucher-Nurminen, 1982; Matile & Widmer, 1993; Gerdes *et al.*, 1999; Berger & Herwegh, 2004). Calcite–dolomite (Cc–Dol) equilibration temperatures (T) were found to be 490–560°C near the forsterite-in isograd, increasing to 480–625°C near the contact at the Cima Uzza summit (Bucher-Nurminen, 1982). Lithostatic pressure (P) during the contact metamorphism has been estimated at ~1 kbar for the Cima Uzza area (Callegari, 1962; McRae, 1982; Brack, 1984), based on stratigraphic reconstructions and phase equilibria. The stable isotope compositions of carbonates indicate limited infiltration of H_2O-rich fluids during contact metamorphism (Gerdes *et al.*, 1995, 1999). Based on the presence of clinozoisite and garnet in the marbles of the underlying Buchenstein formation, Gerdes *et al.* (1995) estimated that the composition of the fluids derived from the intrusive rocks had an $X(CO_2)$ value $<0{\cdot}01$.

On the western flank of Cima Uzza, excellent contacts between mafic intrusive igneous rocks and dolomite are exposed (Fig. 1b). The mafic rocks line the boundary of the main intrusion, which itself is a tonalite (Fig. 1). Based on dating and on field relations, previous studies in this area have argued that the mafic rocks, consisting mainly

of diorites (with a plagioclase composition of $An_{30–40}$), are older than the main intrusive mass (Callegari & Dal Piaz, 1973; Brack, 1984; von Blanckenburg *et al.*, 1998). The mafic intrusions consist of several masses up to 50 m in size, forming stocks and dykes.

The outcrop studied contains up to 30% igneous rocks (Fig. 1b). A 4 m × 6 m carbonate outcrop is partially surrounded by a mafic dyke-like intrusion (Figs 1b and 2). Brucite pseudomorphs after periclase occur in the rim of the carbonate towards the intrusion. They are separated from the non-reacted dolomite by a sharp boundary. The field data show near-complete reaction for all samples within the periclase zone (as will be discussed below), but the zone where periclase decreases from >70% of possible reaction progress to <1% is only a few millimetres thick, which corresponds to about one grain diameter. Periclase rim thicknesses are highly variable at other contacts (from <0·01 m to 4 m), both in dolomite xenoliths and reacted dolomite along the outside contact of the intrusion. Nevertheless, there are some small xenoliths (<1 m) that maintain their central part unchanged.

ANALYTICAL METHODS

Two profiles approximately perpendicular to the contact between the dolomite and the mafic intrusion were sampled. A total of seven samples were investigated in detail (Table 1).

Stable isotope compositions of carbonates were analyzed with a Thermoquest-Finnigan Gas Bench linked to a DeltaPlus XL mass spectrometer at the University of Lausanne following the procedure of Spoetl & Vennemann (2003). Drilled bulk-rock powders were reacted at 90°C for 1 h with concentrated H_3PO_4, and CO_2 was extracted in a stream of He carrier gas. Measured values for $\delta^{13}C$ (VPDB) and $\delta^{18}O$ (VSMOW) were calibrated relative to those of NBS-19.

Calcite compositions for Cc–Dol thermometry were analyzed with a Cameca SX50 electron microprobe (EMP) at the University of Lausanne. Sample current was 6 nA at 15 kV, using a beam diameter of 10 μm. A counting time of 60 s was used for Ca and Fe, and 120 s for Mg and Mn. Natural calcite (Ca), dolomite (Mg), siderite (Fe), and pyrophanite (Mn) was used for standardization. The confidence limit for the Mg values is ∼0·06 wt %, resulting in an analytical error of roughly ± 5°C for the calculated temperatures. Temperatures were calculated using the mean value plus 2σ following Müller *et al.* (2008), and the calibration of Anovitz *et al.* (1987).

Three-dimensional (3D) information on the spatial distribution of periclase in the marbles was obtained by X-ray micro-computed tomography (μ-CT). Cores of 3 mm diameter were drilled out of the samples with a diamond drill. Images with a resolution of 3·9 μm (per pixel) were obtained. Analyses were performed with a Skyscan 1072 μ-CT instrument at the University of Lausanne. The Aphelion© digital image processing software was used to determine the number, size, volume, and 3D distribution of brucite pseudomorphs in the cores. Image analyses were performed on at least three sets of images with a stack height of ∼0·3 mm for each sample. Measured 3D data have been shown to be reproducible with different stacks of images of the same core. The total number of grains was normalized to 1 cm^3. To obtain the original grain size of periclase, the diameters of brucite pseudomorphs (molar volume of 24·63 cm^3/mol) were corrected for the volume change of the retrograde reaction, which forms brucite from periclase (molar volume of 11·25 cm^3/mol), using the volume factor of 0·457.

Table 1: Mineral modes of the brucite-bearing marbles

Sample	Distance from from igneous contact (cm)	Modal percentage		
		dolomite	brucite	calcite
04-TAD-51	20	20·2	34·3	45·5
04-TAD-52	40	29·7	31·6	39·7
04-TAD-47	120	32·0	27·2	40·8
04-TAD-50	130	32·2	28·7	39·1
04-TAD-48	140	22·3	31·5	46·2
04-TAD-54	140	28·4	34·4	37·2
04-TAD-57	200	43·5	26·5	30·0

RESULTS

Petrology

The outcrop described in this study exposes a carbonate, which is in contact with a mafic intrusion on at least two sides (Fig. 2). The other sides are covered by grass. The gray marble distal to the igneous contact consists of pure dolomite with an average grain size of 0·5 mm in diameter. The white dolomite marble closer to the igneous contact is a massive and highly recrystallized marble. The mineral assemblage in these rocks is dolomite + calcite + brucite (Table 1). The idiomorphic, spherical shape of the pseudomorphs indicates that they are pseudomorphs after periclase (Fig. 3). Brucite pseudomorphs appear to be homogeneously distributed, judging from thin sections and μ-CT images (Figs 3 and 4). Periclase was produced above 605°C at an estimated P of 1 kbar, probably in the presence of a water-rich fluid phase, by the reaction (Fig. 5)

$$\begin{aligned} CaMg(CO_3)_2 &\leftrightarrow MgO + CaCO_3 + CO_2. \\ \text{dolomite} &\leftrightarrow \text{periclase} + \text{calcite} + CO_2 \end{aligned} \quad (1)$$

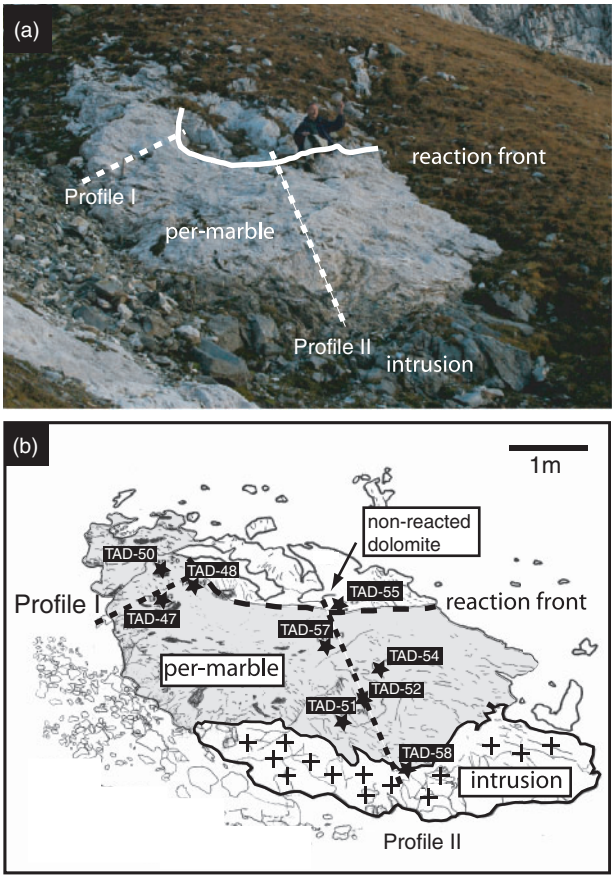

Fig. 2. Seven carbonate and two igneous samples were collected from a 4 m × 6 m marble outcrop as a function of distance from the igneous contact. (a) Photograph of the outcrop. The brucite marble is light coloured, the non-reacted dolomite is darker gray. (b) Sketch of the outcrop showing the sample positions.

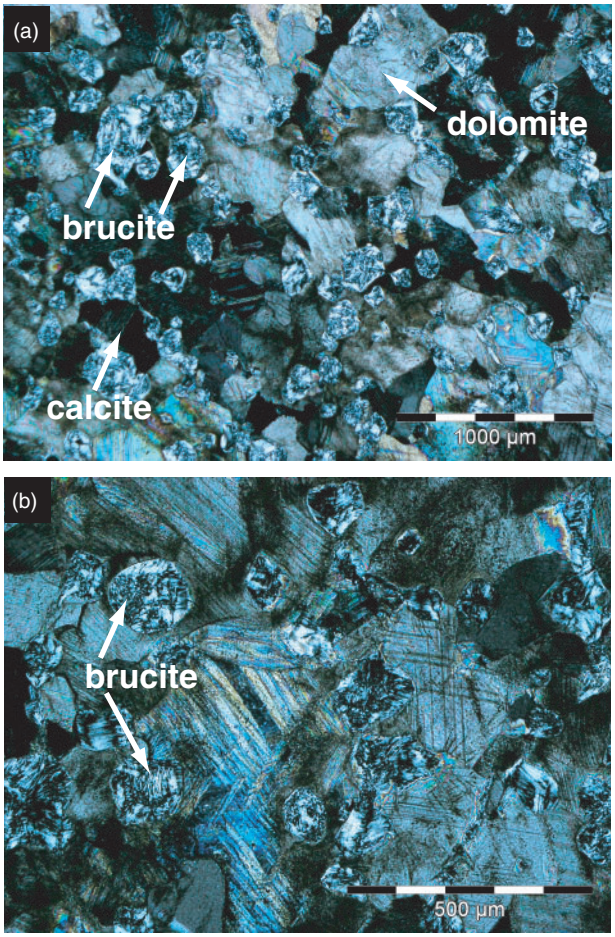

Fig. 3. Photomicrographs of thin sections from the periclase zone, cross-polarized light. Spherical brucite pseudomorphs replacing periclase have grain sizes of up to 200 µm in diameter. (a) and (b) are the two different magnifications of sample 04-TAD-50. (Note the straight grain boundaries of the carbonate crystals.)

Brucite then formed by hydration of periclase on the retrograde path:

$$\begin{gathered} MgO + H_2O \leftrightarrow Mg(OH)_2. \\ \text{periclase} + \text{water} \leftrightarrow \text{brucite} \end{gathered} \quad (2)$$

The progress of reaction (1) was estimated by measuring the volume fraction of brucite in the tomography images. These volume fractions of brucite were converted to volume fractions of periclase by correcting for the volume change accompanying the replacement of periclase by brucite [reaction (2)], assuming a closed system for all oxides with the exception of H_2O.

The measured volume of grains will depend on the choice of the grey-scale threshold used for grain separation on the images. The uncertainties introduced can be large for complex digital image analyses of rock textures. Measured volumes of small objects of only a few pixels in diameter are especially sensitive to these choices. Based on experiments choosing different thresholds for the X-ray images, the radius of selected grains can vary by one or two pixels. As a result, the uncertainty in the measured volume fraction of periclase could be significant, as shown by the error bars in Fig. 6. An evaluation of the actual size of the error is difficult, as grey-scale contrast and crystal size, as well as heterogeneity of the samples would need to be considered. Nevertheless we believe that this procedure probably overestimates the uncertainty. In any case, the measured volume fractions of periclase in all samples are similar within the uncertainty, and reaction progress exhibits no obvious correlation with distance from the intrusion (Fig. 6).

Dolomite is present in all samples. Retrograde dolomite forming haloes surrounding brucite pseudomorphs is observed only in sample 04-TAD-51 (Fig. 7), which is located nearest the igneous contact. In the other samples dolomite crystals have straight, clean grain boundaries

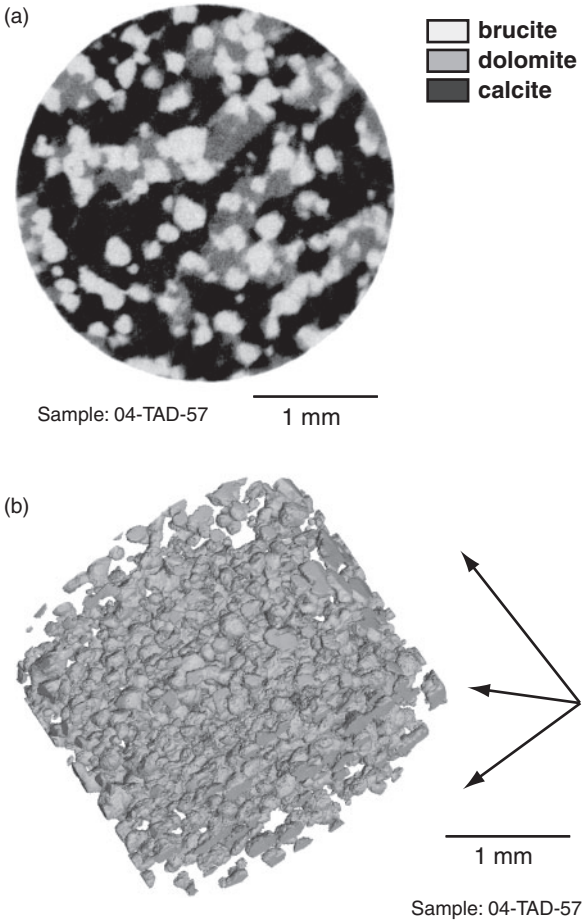

Fig. 4. (a) Typical X-ray μ-CT image of a reacted carbonate sample (04-TAD-57). (Note the absence of retrograde dolomite haloes surrounding the brucite pseudomorphs.) (b) A 3D reconstruction of periclase distribution in a single analyzed core. Brucite crystals are uniformly distributed in three dimensions, indicating pervasive flow of reactive fluid.

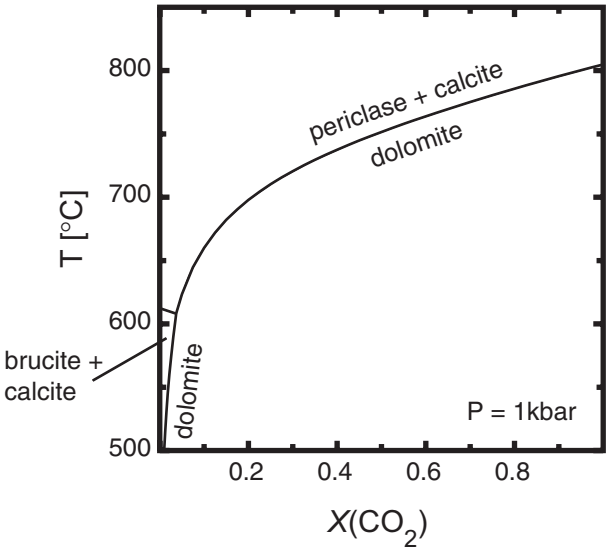

Fig. 5. Phase diagram for the system $CaO–MgO–H_2O–CO_2$ at 1 kbar, calculated using the Perplex software package (Connolly, 1990) and the database of Holland & Powell (2001). $X(CO_2)$ is the mole fraction of CO_2 in a binary $H_2O–CO_2$ fluid phase. Prograde periclase formation takes place above 605°C, initially at water-rich conditions.

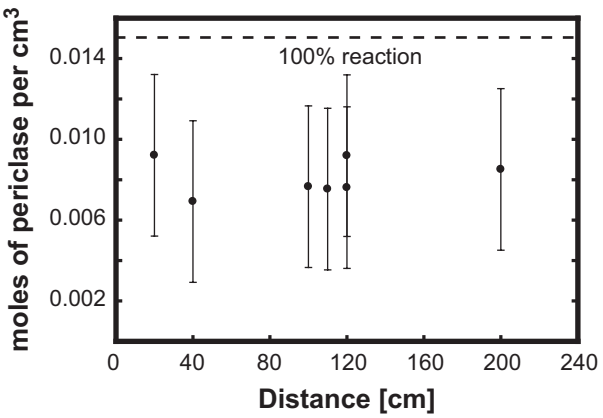

Fig. 6. Diagram showing the reaction progress based on the back-calculated amount of periclase as a function of the distance from the intrusion. No correlation is evident and therefore all samples experienced a similar amount of reaction.

with both calcite and brucite in thin section (Fig. 3) and BSE images (Fig. 7). The large dolomite grains can also be recognized in the X-ray tomography images (Fig. 4). These textures indicate that the dolomite grains are non-reacted original grains.

Calcite–dolomite thermometry

Calcite compositions were measured by EMP in six samples of the periclase skarn (Table 2). Cc–Dol thermometry (Table 3) indicates temperatures between 544°C and 591°C. There is no correlation between calculated temperatures and the distance from the igneous contact. Calcite is a metamorphic product of reaction (1) and should record the temperature of periclase formation. However, most of the calculated values are significantly too low to represent metamorphic peak temperatures. Only the highest calculated values are near the minimum of 605°C required to form periclase based on the equilibrium phase diagram (Fig. 5).

Stable isotopes

Stable isotope compositions for oxygen and carbon were obtained for bulk carbonate samples (Table 4). Within about 40 cm of the igneous contact, the marbles are significantly depleted in $^{18}O/^{16}O$ and $^{13}C/^{12}C$ to $\delta^{18}O$ and $\delta^{13}C$ values of $14{\cdot}6 \pm 0{\cdot}1$‰ (VSMOW) and $-3{\cdot}2 \pm 0{\cdot}05$‰ (VPDB), respectively. Both $\delta^{18}O$ and $\delta^{13}C$ values increase rapidly with increasing distance from the magmatic

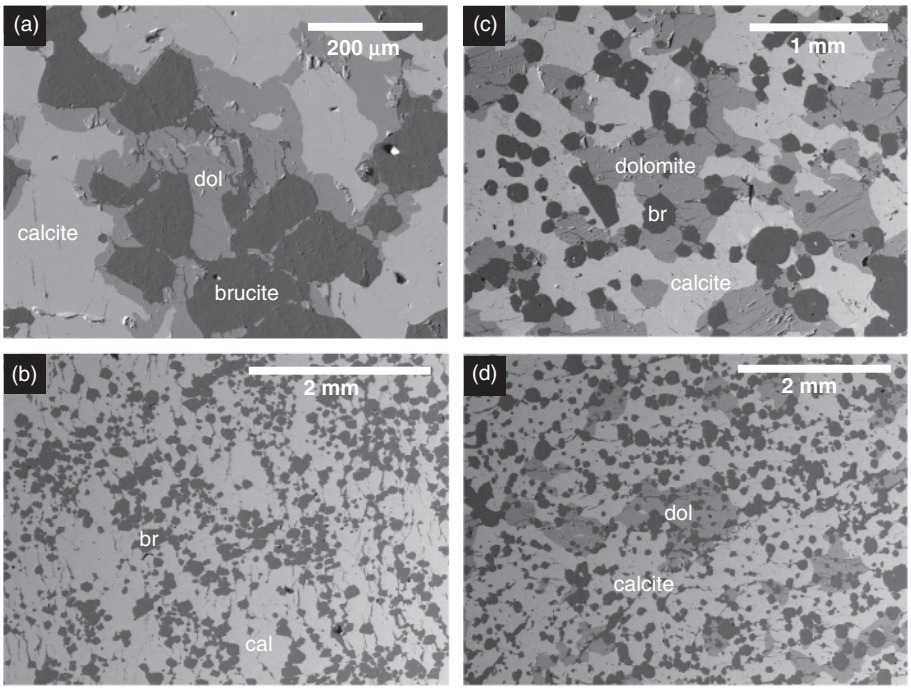

Fig. 7. BSE images of two carbonate samples. (a, b) Sample 04-TAD-51. Small retrograde dolomite haloes are found only near the igneous contact. (c, d) Sample 04-TAD-47. Prograde dolomite in samples further away exposes original large grains.

Table 2: Representative calcite analyses from the studied marbles of Cima Uzza (Adamello Massif, Italy)

	04-TAD-47	04-TAD-50	04-TAD-48	04-TAD-51	04-TAD-52	04-TAD-57
CaO	52·88	51·99	51·79	53·57	53·06	53·74
MgO	1·77	1·82	1·72	2·23	1·66	1·68
MnO	0·00	0·00	0·00	0·00	0·00	0·00
FeO	0·07	0·00	0·00	0·06	0·00	0·06
Mineral formula						
$Ca(CO_3)$	0·955	0·954	0·956	0·944	0·958	0·957
$Mg(CO_3)$	0·044	0·046	0·044	0·055	0·042	0·042
$Fe(CO_3)$	0·000	0·000	0·000	0·000	0·000	0·000
$Mn(CO_3)$	0·001	0·000	0·000	0·000	0·000	0·001

Analyses were obtained using a 15 keV, 6 nA, 10 μm beam. Mineral formulae were calculated based on $(Ca + Mg + Fe + Mn) = 1$.

contact (Fig. 8) to values of ~28‰ and about −1·0‰, respectively, defining sharp isotope exchange fronts for both C and O. Gerdes *et al.* (1999) found similar C and O values and spatial patterns in brucite marbles near mafic dykes on the southern slopes of Cima Uzza. The isotope exchange fronts for C and O are located at the same distance from the contact (Fig. 8), pointing to the same amount of exchange for C and O. This equivalence in turn would imply an infiltrating fluid composition of $X(CO_2) = 0{\cdot}5$ assuming local equilibrium or similar reaction kinetics for O and C exchange (e.g. Baumgartner & Rumble, 1988; Baumgartner & Valley, 2001).

Crystal size distributions (CSD)

The X-ray tomography measurements reveal that the brucite crystals are homogeneously distributed in three dimensions in all analyzed cores (Figs 4 and 9). No obvious clustering is observed on the images and the crystals are not aligned on planes that could correspond to annealed fractures. In addition, the absence of apparent veins indicates that fluid flow was pervasive. The data obtained by μ-CT are listed in Table 5. The CSDs indicate that the brucite pseudomorphs range in size from 20 to 200 μm in diameter in all samples. CSDs for all samples are calculated using a bin size of 20 μm; this size is based on the estimated uncertainty of the image analyses. Given this uncertainty, the X-ray tomography measurements do not consistently detect or measure reliably the sizes of grains smaller than 20 μm.

CSDs represent the number of crystals (n) within specified size intervals (bin sizes) per unit volume. They are typically plotted as crystal population density on a logarithmic scale (ln n density) vs grain size. Measured CSDs change as a function of their distance from the igneous contact (Fig. 9). The CSDs for the samples along the

Table 3: Calcite–dolomite thermometry data determined for selected brucite marbles

Sample	No. of analyses	Distance to next visible contact (cm)	*X*Mg			Peak temperature (°C)	
			Max.	Mean	SD	Calculated with mean + 2σ	Calculated using the highest *X*Mg value
04-TAD-47	124	120	0·064	0·043	0·008	562	578
04-TAD-48	128	140	0·059	0·043	0·007	554	561
04-TAD-50	124	130	0·069	0·046	0·009	577	593
04-TAD-51	145	20	0·068	0·052	0·008	590	591
04-TAD-52	142	40	0·060	0·043	0·006	549	562
04-TAD-57	146	200	0·059	0·042	0·006	544	562

Table 4: Summary of O and C stable isotope compositions for bulk-rock powders of carbonate samples from the southern Adamello Massif, Italy

Sample	Distance (m)	$\delta^{13}C$ (VPDB) (‰)	$\delta^{18}O$ (VSMOW) (‰)
04-TAD-46	0·2	−2·2	24·0
04-TAD-47	1·2	−1·0	28·5
04-TAD-48	1·4	−1·3	28·5
04-TAD-50	1·3	−1·4	27·7
04-TAD-51	0·2	−2·6	20·1
04-TAD-52	0·4	−1·3	28·3
04-TAD-54	1·4	−1·2	28·2
04-TAD-55	2	−1·1	28·0
04-TAD-56	4·5	−0·8	26·4
04-TAD-57	1·7	−1·4	27·9
04-TAD-58	0·1	−3·2	14·6

profiles are superimposed on one another in Fig. 10 for comparison. It can be seen that the CSDs of brucite pseudomorphs become flatter (i.e. slopes decrease) with increasing distance from the contact. This trend can be observed for both profiles, and occurs because there are progressively larger variations in the size of pseudomorphs and increasing abundance of larger grains in samples further from the contact (Figs 9–11). As a consequence, the number of grains per unit volume (n) decreases with increasing distance from the contact. This trend is verified by a plot of the calculated number of grains per unit

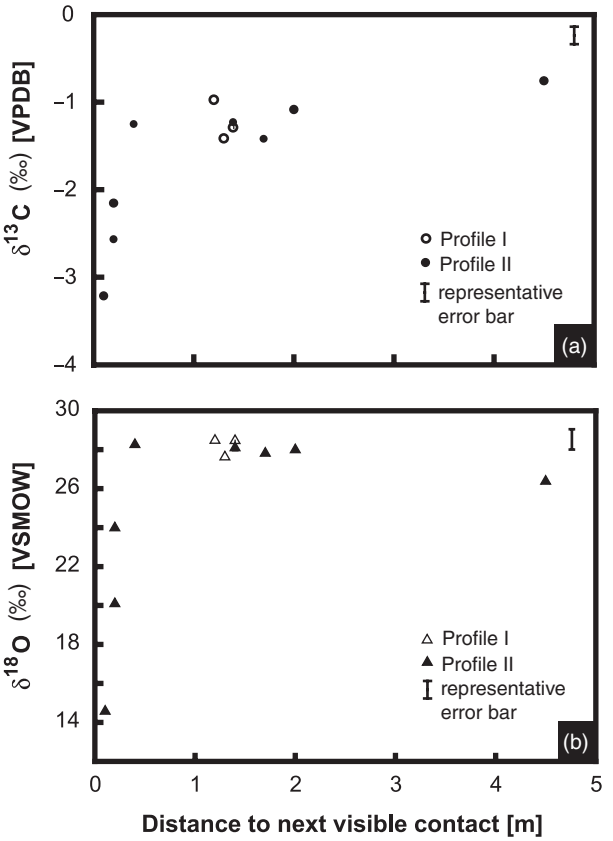

Fig. 8. Measured isotope compositions for carbon (a) and oxygen (b) of bulk carbonate from the Cima Uzza samples. Depletion of $^{13}C/^{12}C$ and $^{18}O/^{16}O$ in the carbonate samples defines sharp C- and O-isotope exchange fronts located near the contact with the mafic intrusion, indicating a limited amount of fluid infiltration. (Note that both fronts are located at the same distance from the contact.)

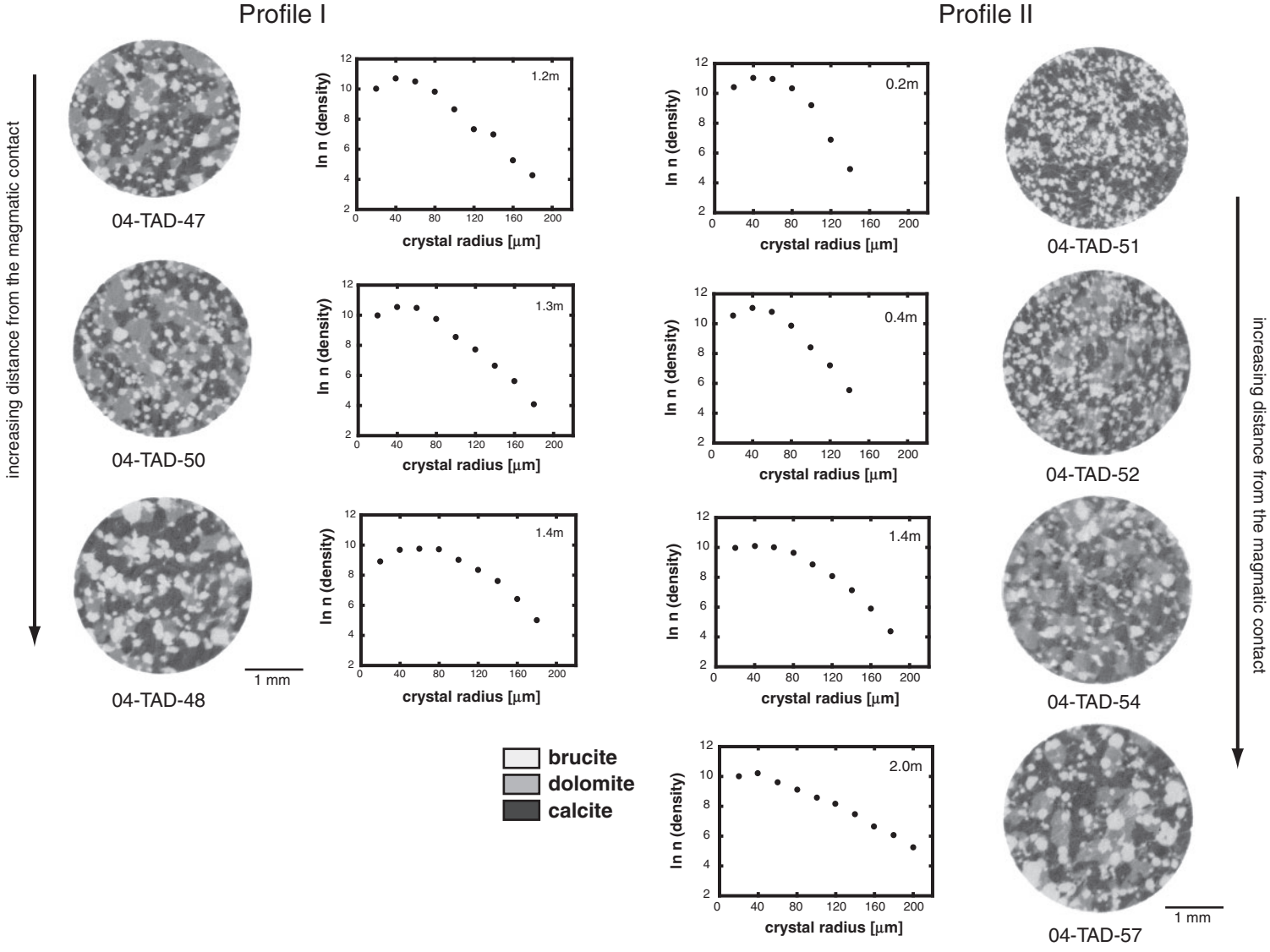

Fig. 9. Typical X-ray μ-CT slice images are shown at the left and right, and measured CSDs for brucite marbles in these samples in the center. With increasing distance from the igneous contact, the CSDs become progressively flatter, indicating on the one hand a decrease in the number of grains and on the other the presence of larger grain sizes in samples at greater distances from the contact.

Table 5: Stereographic data for periclase pseudomorphs, not corrected for volume change caused by hydration to brucite, obtained by computed X-ray microtomography

Sample	Distance (cm)	$V_{analyzed}$ (cm^3)	No. of grains detected	$V_{brucite}$ (cm^3)	Average sphericity	Median radius (μm)
04-TAD-51	20	1·29E–02	2477	3·30E–03	0·67	53
04-TAD-52	40	1·32E–02	2220	2·20E–03	0·68	46
04-TAD-47	120	1·05E–02	1361	2·10E–03	0·71	51
04-TAD-50	130	1·28E–02	1529	2·40E–03	0·72	53
04-TAD-48	140	1·07E–02	743	2·50E–03	0·64	73
04-TAD-54	140	1·32E–02	1206	2·50E–03	0·67	54
04-TAD-57	200	1·28E–02	1052	2·70E–03	0·74	57

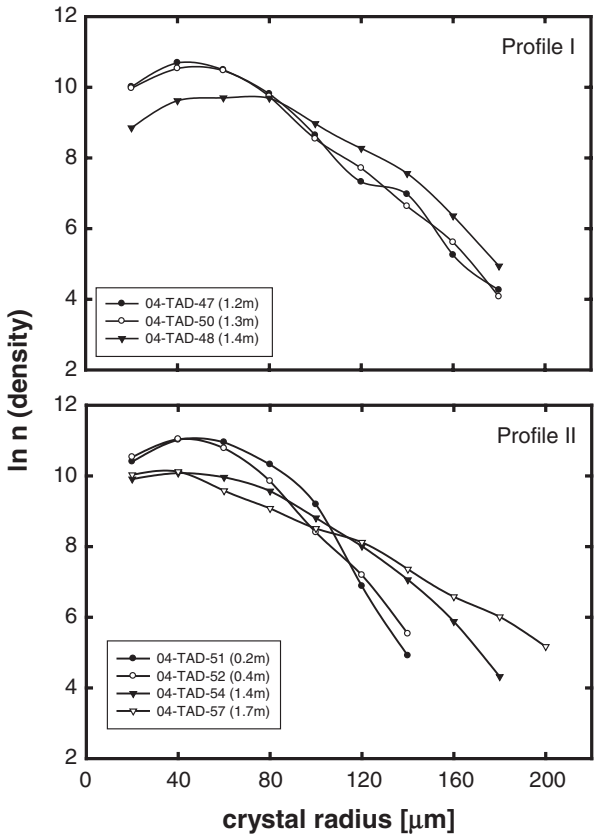

Fig. 10. CSDs of periclase from the two sampled profiles. (Note that the CSDs become flatter with increasing distance from the igneous contact.)

volume vs distance from the igneous contact (Fig. 12). Despite these trends, the median grain size (40–60 μm radius) remains approximately the same along both profiles (Table 5).

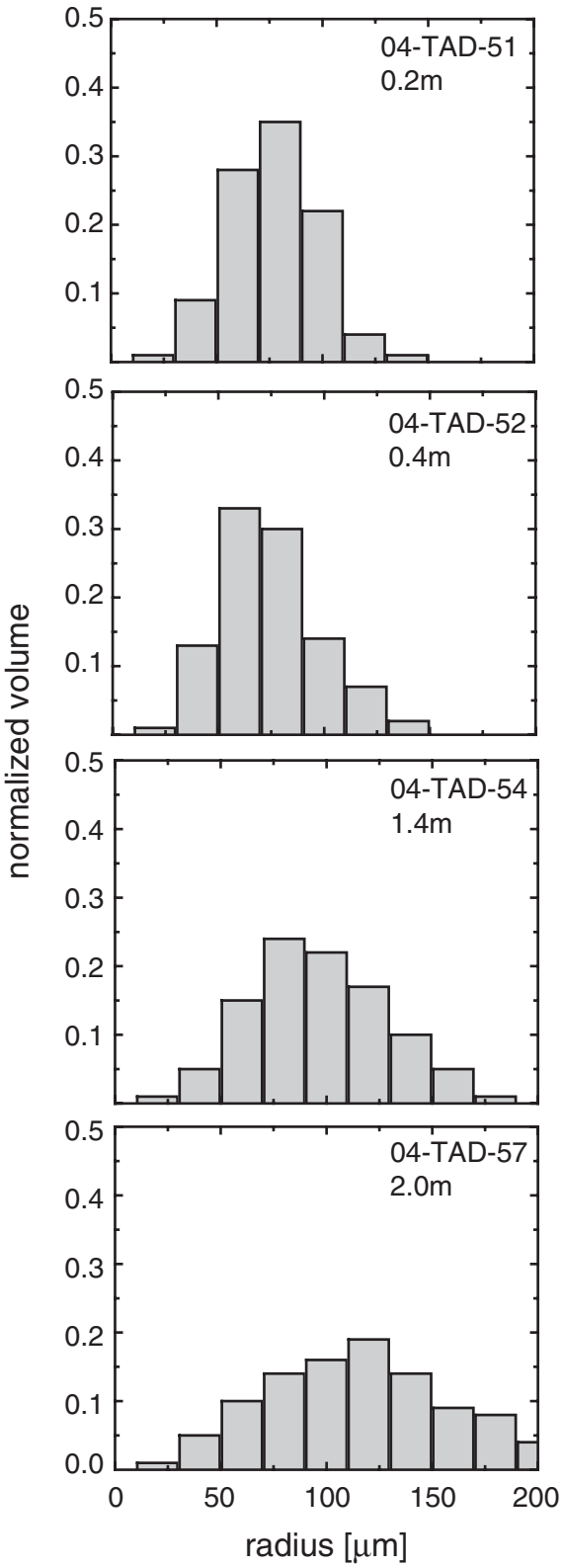

Fig. 11. Frequency–volume plot illustrating the volume proportions of different grain sizes (radius) in the analyzed cores. Samples at increasing distance from the igneous contact exhibit progressively larger proportions of larger grains indicating higher growth rates compared with nucleation rates.

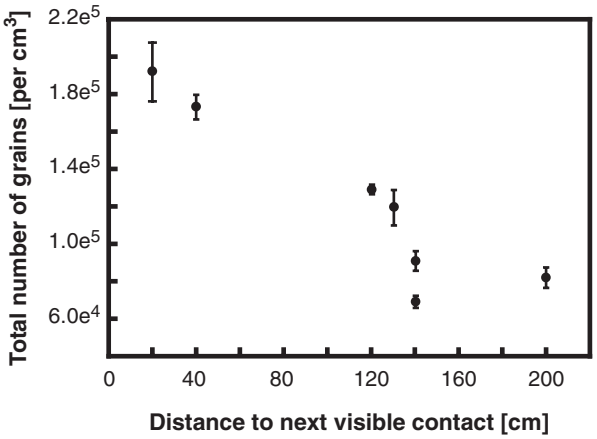

Fig. 12. Plot of the total number of grains, normalized to 1 cm^3 of rock, as a function of the distance from the contact with the intrusion. The number of grains decreases continuously with increasing distance.

DISCUSSION

At the estimated lithostatic pressure of 1 kbar, phase equilibria require formation of periclase at minimum temperatures at 605°C (Fig. 5) and a water-rich fluid phase. Progressively higher temperatures are required to form periclase as the CO_2 content of the pore fluid increases, to $T > 780$°C in pure CO_2 fluid, when periclase could form without fluid infiltration. Thus, formation of periclase could also be explained by a simple thermal activated reaction if the marbles were heated to sufficiently high temperatures. Indeed, the igneous temperatures of the diorites are estimated at 800–850°C, sufficiently high to cause a thermally driven reaction if the mass of surrounding igneous rocks is large enough and igneous rocks surround the carbonates. In contrast, the geology illustrated in Fig. 1b suggests that this is not an area of small single xenoliths in an ocean of magma. Indeed, the outcrop is located at the border of the heavily intruded area close to the summit of Cima Uzza. The absence of detailed knowledge about the relative timing of the various events of magma intrusion makes it very difficult to fully describe the thermal regime. However, simple heat balance and transport considerations, based on the observed sub-equal amounts of intrusion and dolomite exposed in the study area, suggest that maximum temperatures achieved during contact metamorphism are much closer to 600–650°C (a reasonable intrusive contact temperature for the diorite magma composition at 1 kbar). Furthermore, purely thermally driven formation of periclase should result in similar ('equal') sizes of reaction rims in each xenolith or pendant, as the thermal diffusivity is roughly the same. In addition, small xenoliths should be totally changed into periclase xenoliths. This is in clear contrast to the field observations, which indicate variable thicknesses of the periclase rims and even the preservation of non-reacted cores in relatively small xenoliths as described above. Taken together, these considerations suggest maximum temperatures of ~650°C. The formation of periclase is hence at least partially driven by infiltration of a fluid phase.

Temperatures measured by Cc–Dol thermometry in this area are up to 600°C (this study; Bucher-Nurminen, 1982) and slightly too low for periclase formation. Several studies have documented similar results for the periclase zone in other contact aureoles (Cook & Bowman, 1994; Müller *et al*. 2008). In contrast, however, various studies have shown that Cc–Dol thermometry can record temperatures significantly above 600°C. Sometimes even values that are too high to be considered realistic were obtained; for example, for the Ubehebe contact aureole (Roselle *et al*., 1999; Müller *et al*. 2008), the Alta contact aureole (Cook & Bowman, 1994), and for Cc inclusions in forsterite (Ferry, 2001). Müller *et al*. (2008) presented a combined growth–diffusion–dolomite unmixing model for calcite in contact aureoles, which explains these observations, and applied it to the Ubehebe contact aureole. Consequently, we believe that the measured temperatures are 10–50°C too low, and represent partially reset values.

Taking together data from geothermometry and the general heat conduction and geometry arguments discussed above, we suggest that periclase was formed at 605–650°C, in excellent agreement with the observations of Bucher-Nurminen (1982). Reaction (1) produces pure CO_2, and hence very little reaction progress can occur at H_2O-rich conditions, unless temperature increases significantly or the amount of CO_2 produced is diluted by an externally derived H_2O-rich fluid. Hence we conclude that infiltration of water-rich fluids was needed to produce the periclase zone. In addition, thermal gradients were less than 50°C during its formation.

Stable isotope data provide additional information on the mechanism driving the metamorphic mineral reactions (e.g. Rumble, 1982; Ferry, 1991; Nabelek *et al*., 1992; Baumgartner & Valley, 2001). The measured $^{13}C/^{12}C$ and $^{18}O/^{16}O$ depletions in the marbles within ~40 cm of the igneous contact require infiltration of a low $\delta^{18}O$ and $\delta^{13}C$ fluid. The source of the isotopic depletion is either the mafic rocks or fluid flowing along the contact between the carbonates, similar to the suggestion of Gerdes *et al*. (1999) for brucite marbles in the summit area of Cima Uzza. The original sedimentary values (Gerdes *et al*., 1999) are maintained at about 80 cm away from the contact. Assuming that the fluid infiltrated perpendicular to the contact along the measured profiles into the carbonates, the short distance of isotope alteration suggests a limited amount of fluid infiltration. Further, the equivalent positions of the C- and O-isotope exchange fronts indicate a fluid composition of $X(CO_2) = 0{\cdot}5$ for the infiltrating fluid (Baumgartner & Valley, 2001). Such a high $X(CO_2)$

fluid composition is incompatible with the phase equilibria, which require H_2O-rich conditions at the preferred temperatures (605–650°C) of periclase formation (Fig. 5). Cathodoluminescence (CL) images obtained on selected samples revealed no zoning, either in single dolomite (indicating retrograde reaction) or calcite crystals. Similarly, no chemical zoning is apparent based on EMP analysis. Consequently, we interpret the absence of such zoning patterns to indicate that the fluid causing the isotopic shift was indeed a high-T fluid (605–650°C), causing mineral reaction, and not a late-stage meteoric fluid ($T < 605$°C) as has been argued for isotope profiles in Naxos (Lewis *et al.*, 1998).

The relative positions of reaction and isotope exchange fronts have been addressed in several studies using simple infiltration models (Baumgartner & Rumble, 1988; Bickle & Baker, 1990; Ferry, 1991). These models assume isothermal infiltration of a fluid with a different isotopic composition into a rock column, whereas local equilibrium is maintained during isotope exchange and mineral reactions. Baumgartner & Rumble (1988) have shown that the advance of the O-isotope front is independent of temperature and the original isotopic composition of the host rock. The equilibrium assumption reduces the calculation of the velocity of the isotope exchange front to a simple mass-balance calculation, dependent on only the cumulative fluid flux and the relative abundance of oxygen in the fluid and the rock, respectively. However, equilibrium $X(CO_2)$ for the periclase-forming reaction increases with increasing temperature (Fig. 5). Because the reaction progress depends on the difference between equilibrium and infiltrating $X(CO_2)$ (Ferry, 1991), the advance of the reaction front will depend not only upon the amount of fluid infiltration and its composition, but also upon the temperature at which infiltration takes place (Ferry & Rumble, 1997; Ferry & Gerdes, 1998).

The temperature required for the observed location of the reaction front to be compatible with the locations of the C- and O-isotope fronts, assuming 1D fluid flow perpendicular to the contact, can be evaluated according to calculations for a simple infiltration model (Korzhinskii, 1965; Frantz & Weisbrod, 1974; Baumgartner & Rumble, 1988). Assuming a rock column of 1 m length and a cross-sectional area of 1 cm^2 consisting of pure dolomite one can calculate the relative positions of the isotope and reaction front as a function of temperature [equilibrium $X(CO_2)$] and infiltrating $X(CO_2)$. Based on the amount of O in the dolomite, the O-isotope front will advance about 9·5 cm per mole of infiltrating pure H_2O fluid. However, an advancement of the reaction front 10 times further than the isotope alteration front (i.e. about 95 cm per mole infiltrating pure water), as observed in the outcrop, requires equilibration of the fluid phase at an $X(CO_2)$ value of 0·6 for reaction (1) by mass balance. This equilibrium $X(CO_2)$ value in turn suggests a temperature of ~760°C for the periclase-forming reaction (Fig. 5). Hence, the relative positions of the reaction and isotope exchange fronts could be explained by infiltration of a limited amount of a water-rich, high-T fluid phase. Nevertheless, this calculated temperature, which has to be regarded as a minimum value as infiltration of essentially pure water was assumed, clearly appears to be too high to be realistic and is in strong disagreement with the thermometry data (Bucher-Nurminen, 1982; this study). Alternatively, the superimposition of the carbon and oxygen isotope fronts could be the result of fluid flow oblique or even perpendicular to the sample traverse (e.g. parallel to the igneous contact; Gerdes *et al.*, 1995). The resulting isotope profiles then represent the side of a propagating infiltration front as suggested by Yardley & Lloyd (1995). Because the principal vector of advection would now be parallel to the igneous contact, the isotope exchange fronts in the measured profile would primarily reflect diffusion and dispersion towards the side. Consequently, the resulting profiles exhibit sharp fronts that are not strongly separated, and that are displaced only a very limited distance from the igneous contact (Gerdes *et al.*, 1995).

In summary, the geometry and the dimension of the outcrop, the sharp reaction front within the xenolith, the Cc–Dol thermometry data (albeit partially reset), and stable isotope compositions suggest a magmatic origin for the fluid phase. The lack of CL zoning patterns argues against significant late re-equilibration of the isotopic compositions of the carbonates.

The simple infiltration models presented above all assume local equilibrium for the mineral reactions. This results in a sharp reaction front regardless of whether fluid transport is assumed to be dominated by diffusion (Frantz & Mao, 1976) or advection (Frantz & Weisbrod, 1974; Baumgartner & Rumble, 1988; Lichtner, 1996). The rock is found to be completely reacted upstream of the front, whereas downstream no reaction occurs. Although the described outcrop exhibits a sharp boundary between brucite marbles and non-reacted carbonate, dolomite is present in all samples from the profiles. Only in the sample closest to the contact are the textures consistent with a retrograde origin for dolomite (Fig. 7). If dolomite in all the other samples is not late (either from retrograde reaction involving periclase or brucite or as a late precipitate), its presence indicates that the periclase reaction did not go to completion, and suggests that reaction kinetics are indeed significant in this case.

The CSDs of periclase provide information on the kinetics of crystallization. Rates for the nucleation and growth of minerals are linked to the reaction affinity (e.g. Rubie & Thompson, 1985; Carlson *et al.*, 1995; Roselle *et al.*, 1997; Lasaga, 1998). The possible relationship between nucleation and growth rates as a function of the reaction affinity

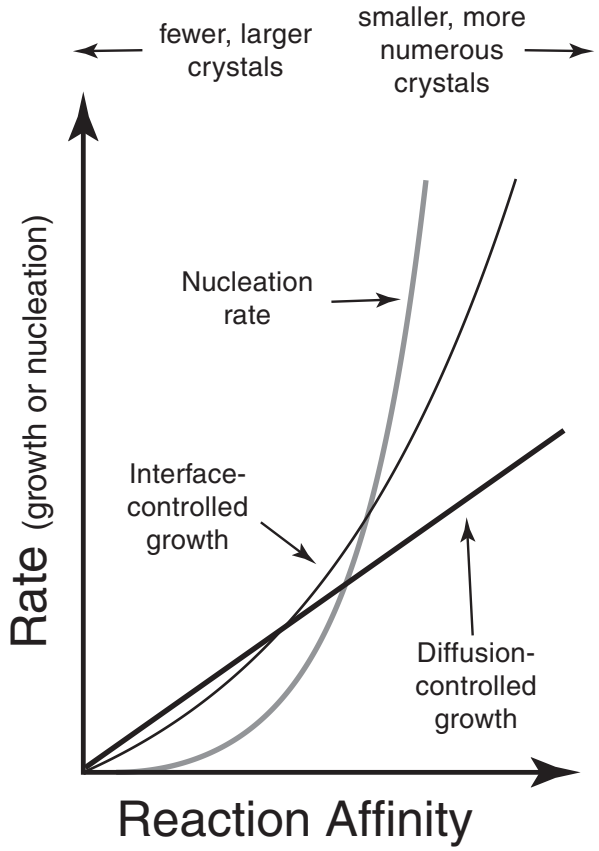

Fig. 13. Schematic plot showing the relationship between nucleation and growth rates as a function of the reaction affinity (from Roselle *et al.*, 1997). For high degrees of overstepping in the case of $X(CO_2)^{eff} \ll X(CO_2)^{eq}$, the nucleation rates are much larger relative to the growth rate, whereas for low reaction affinities growth rates are higher than nucleation rates.

is schematically shown in Fig. 13. The reaction affinity for the periclase-forming reaction is given by

$$\Delta G = -RT \ln\left(\frac{X_{CO2}^{eff}}{X_{CO2}^{eq}}\right). \quad (3)$$

In equation (3), R is the universal gas constant, $X(CO_2)^{eff}$ is the actual mole fraction of CO_2 in the fluid phase, and $X(CO_2)^{eq}$ is the equilibrium $X(CO_2)$ value. Here we neglected possible temperature gradients, for simplicity.

A kinetic model is shown schematically in Fig. 14a, where an H_2O-rich fluid infiltrates a rock column of dolomite with an arbitrarily chosen equilibrium value for $X(CO_2)$ at a constant temperature, creating an infiltration front. The actual interplay of advection, diffusion and reaction will determine the exact advance and shape of the infiltrating front. The actual reaction affinity for the system at a given position and time is roughly proportional to the deviation of the effective $X(CO_2)$ value from its

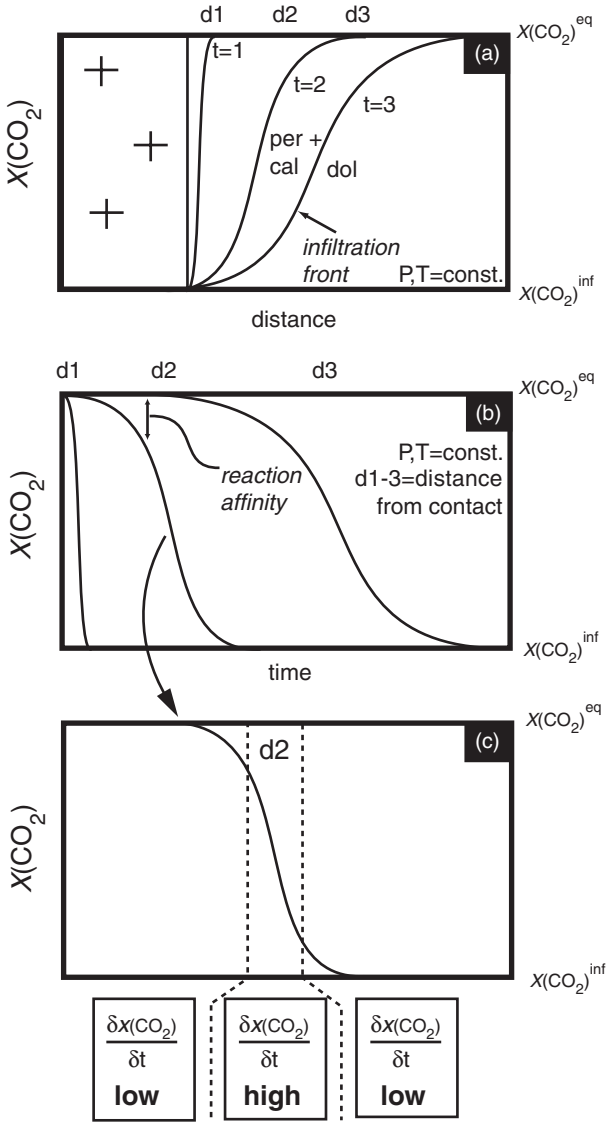

Fig. 14. (a) Qualitative model for isothermal infiltration of a disequilibrium fluid into a dolomite rock. (b) Evolution of the shape of the infiltration front with time. (c) Reaction affinity scale with the deviation from the equilibrium $X(CO_2)$ value. Large changes in $X(CO_2)$ can cause large reaction affinities. Rampant nucleation is the result.

equilibrium value with time as illustrated in Fig. 14b and c. As the front advances through the column over time, the contributions of diffusion, dispersion, and reaction kinetics will progressively broaden the front. The reaction affinity profile will hence also broaden, increasing the length of time favorable for growth and increasing differences in rates of change in reaction affinity [slope $\partial X(CO_2)/\partial t$] with time. At the initial stage the front is very sharp, causing a rapid change in $X(CO_2)$. The resulting increase to high reaction affinities will produce high nucleation rates when compared with growth rates (Fig. 14a). Consequently, a large quantity of periclase

crystals will nucleate over a very short time span and start to grow rapidly. Thus, a restricted CSD with high proportions of similar grain sizes, consistent with a surface-controlled growth mechanism (Carlson & Denison, 1992), is predicted (Fig. 15b).

The reaction kinetics, diffusion and dispersion will successively flatten the front with time and the change in $X(CO_2)$, $\partial X(CO_2)/\partial t$, decreases (Fig. 14b). During the initial stage of reaction this smaller spatial gradient in CO_2 concentration will allow fewer periclase crystals to nucleate over the same time interval, as a result of the smaller rate of increase in reaction affinity. Subsequent increase in slope, $\partial X(CO_2)/\partial t$, for the next time interval of reaction will increase reaction affinity, which will increase the nucleation rate and allow a relatively large number of crystals to nucleate over a relatively short time interval. The resulting population of crystals would include some early, large crystals and a relatively large number of younger crystals of similar size (Fig. 15c). At progressively later times (greater distances), the maximum slope of the reaction affinity–time profile for this intermediate stage of growth decreases again, expanding the time interval for nucleation and growth but decreasing the rates of increase in nucleation (Figs 14c and 15d). Hence, samples at progressively greater distance from the igneous contact can exhibit similar sizes for the majority of periclase crystals but also contain progressively greater fractions of larger grains, reflecting the early nucleated grains, which subsequently had more time to grow (Fig. 15c and d). Further, CSDs will become progressively flatter with increasing distance from the magmatic contact, reflecting the overall longer time interval of growth (Fig. 10). All these changes are observed in the CSD diagrams (Figs 9–12).

The reactive surface area of the reactant dolomite is another parameter controlling the reaction rate for the periclase-forming reaction. Progressive consumption of dolomite will decrease its reactive surface area and thus also decrease the rate of reaction. A simple rate law is given by the equation

$$\text{rate} = S_A\, K \left[1 - \left(\frac{X^{\text{eff}}_{CO2}}{X^{\text{eq}}_{CO2}}\right)\right] \qquad (4)$$

where S_A is the reactive surface area of the rate-limiting mineral, and K is the kinetic constant. In addition, the surfaces of dolomite grains can potentially be isolated during progressive reaction, although fluid infiltration was pervasive. These two effects could potentially stop or at least significantly slow down the reaction, preserving remnant dolomite in parts of the rock.

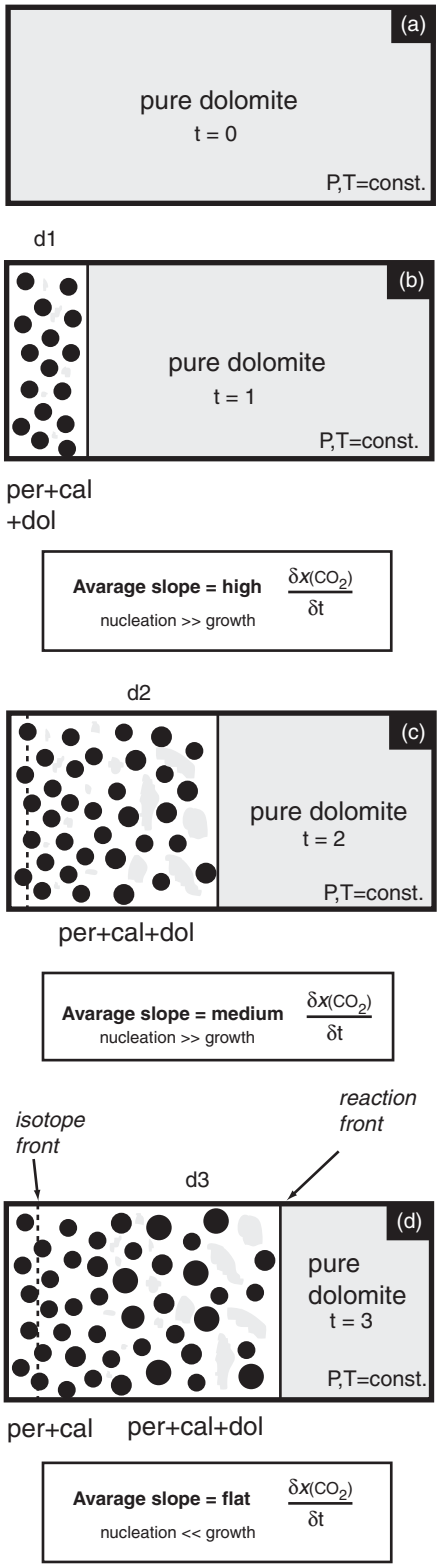

Fig. 15. Schematic sketch of the advancement of reaction and isotope exchange fronts, as well as nucleation and growth as function of time. (a) Prior to infiltration the rock is composed of pure homogeneous dolomite grains. (b) At an initial stage, infiltration causes large changes in $X(CO_2)$, resulting in high reaction affinities. As a result the nucleation rate is higher than the growth rate and many small, similar-sized grains are formed. (c, d) Subsequently, the slope of the infiltration front becomes flatter, resulting in smaller reaction affinities. Growth rates increase and result in a greater proportion of larger grains.

CONCLUSIONS

Brucite pseudomorphs in contact metamorphic marbles in xenoliths near the Cima Uzza summit of the southern

Adamello Massif are the result of retrograde replacement of periclase crystals. Prograde formation of periclase crystals in these marbles is the result of high-temperature disequilibrium infiltration of H_2O-rich fluids. The short distance of $^{13}C/^{12}C$ and $^{18}O/^{16}O$ depletion and the coincidence of the C and O isotopic fronts indicate either a relatively small flux of infiltrating fluid with an $X(CO_2) = 0{\cdot}5$ normal to the igneous contact or that the infiltration front was oblique to the sample profiles. Although there is a sharp boundary separating the brucite marbles from non-reacted dolomite, reactant dolomite is still present in most samples of brucite marble. The incomplete periclase reaction is interpreted to be the result of kinetically controlled mineral growth at near-isothermal conditions. Progressive reaction may sufficiently decrease the kinetics by decreasing the reactive surface area of dolomite, isolating its crystal surfaces to reduce the rate, or perhaps even to stop the periclase reaction, leaving reactant dolomite in most samples. The reaction affinity in the system is controlled by the shape of the fluid infiltration front. As diffusion and dispersion become more effective with increasing distance from the magmatic contact, the infiltration front and reaction affinity profile broaden progressively. As a result, the reaction affinity will increase more slowly at progressively later positions of the reaction front, yielding initially lower nucleation and growth rates, smaller changes in nucleation and growth rates, but longer time intervals for growth. The results are progressively broader grain size distributions, including greater proportions of larger periclase crystals with increasing distance from the igneous contact but a smaller number of grains. Hence, this interpretation is compatible with the CSDs measured for both profiles in this study (Figs 9–12).

ACKNOWLEDGEMENTS

This study is part of the first author's Ph.D. thesis. Comments and discussions with M. Cosca and T. W. Vennemann on earlier versions of the manuscript are gratefully acknowledged. Financial support was provided by grant 2100-066996 from the Swiss National Science Foundation. Insightful reviews by S. Penniston-Dorland, B. Yardley, D. Jerram, and M. Herwegh helped us to improve the clarity of the paper significantly. B. Grobéty, P. Ulmer and A. Wohlers are thanked for their help in obtaining the original geological maps of the Cima Uzza area. We also thank R. Gieré for the editorial handling.

REFERENCES

Albarède, F. & Bottinga, Y. (1972). Kinetic disequilibrium in trace-element partitioning between phenocrysts and host lava. *Geochimica et Cosmochimica Acta* **36**, 141–156.

Anovitz, L. M., Essene, E. J., Goldsmith, J. R. & Heard, H. C. (1987). Phase equilibria in the system $CaCO_3$–$MgCO_3$–$FeCO_3$. *Journal of Petrology* **28**, 389–414.

Baumgartner, L. P. & Rumble, D. (1988). Transport of stable isotopes. 1. Development of a kinetic continuum theory for stable isotope transport. *Contributions to Mineralogy and Petrology* **98**, 417–430.

Baumgartner, L. P. & Valley, J. W. (2001). Stable isotope transport and contact metamorphic fluid flow. In: Valley, J. W. & Cole, D. R. (eds) *Stable Isotope Geochemistry. Mineralogical Society of America, Reviews in Mineralogy and Geochemistry* **43**, 415–467.

Berger, A. & Herwegh, M. (2004). Grain coarsening in contact metamorphic carbonates: effects of second-phase particles, fluid flow and thermal perturbations. *Journal of Metamorphic Geology* **22**, 459–474.

Bickle, M. & Baker, J. (1990). Migration of reaction and isotopic fronts in infiltration zones: assessments of fluid flux in metamorphic terrains. *Earth and Planetary Science Letters* **98**, 1–13.

Brack, P. (1984). *Geologie der Intrusiva und Rahmengesteine des Suedwest-Adamello (Nord-Italien)*. Zürich: Eidgenössisch Technische Hochschule.

Bucher-Nurminen, K. (1982). On the mechanism of contact aureole formation in dolomitic country-rock by the Adamello intrusion (northern Italy). *American Mineralogist* **67**, 1101–1117.

Callegari, E. (1962). *La Cima Uzza (Adamello Sud-Orientale). Parte I. Studio petrografico e petrogenetico delle formazioi metamorfiche di contatto*. Padova: University of Padova, 116 p.

Callegari, E. & Dal Piaz, G. B. (1973). Field relationships between the main igneous masses of the Adamello Intrusive Massif (N. Italy). *Memorie degli Istituti Geologia e Mineralogia dell'Università di Padova* **24**, 1–38.

Carlson, W. D. & Denison, C. (1992). Mechanisms of porphyroblast crystallization: results from high-resolution computed X-ray tomography. *Science* **257**, 1236–1239.

Carlson, W. D. & Gordon, C. L. (2004). Effects of matrix grain size on the kinetics of intergranular diffusion. *Journal of Metamorphic Geology* **22**, 733–742.

Carlson, W. D., Denison, C. & Ketcham, R. A. (1995). Controls on the nucleation and growth of porphyroblasts: kinetics from natural textures and numerical models. *Geological Journal* **30**, 207–225.

Carlson, W. D., Denison, C. & Ketcham, R. A. (1999). High-resolution X-ray computed tomography as a tool for visualization and quantitative analysis of igneous textures in three dimensions. *Visual Geosciences* **4**, 3.

Cashman, K. V. & Ferry, J. M. (1988). Crystal size distribution (CSD) in rocks and the kinetics and dynamics of crystallization. 3. Metamorphic crystallization. *Contributions to Mineralogy and Petrology* **99**, 401–415.

Cashman, K. V. & Marsh, B. D. (1988). Crystal size distribution (CSD) in rocks and the kinetics and dynamics of crystallization. 2. Makaopuhi Lava Lake. *Contributions to Mineralogy and Petrology* **99**, 292–305.

Colombo, A. & Tunesi, A. (1999). Pre-Alpine metamorphism of the Southern Alps west of the Giudicarie Line. *Schweizerische Mineralogische Und Petrographische Mitteilungen* **79**, 63–77.

Connolly, J. A. D. (1990). Multivariable phase-diagrams—an algorithm based on generalized thermodynamics. *American Journal of Science* **290**, 666–718.

Cook, S. J. & Bowman, J. R. (1994). Contact-metamorphism surrounding the Alta Stock—thermal constraints and evidence of advective heat-transport from calcite plus dolomite geothermometry. *American Mineralogist* **79**, 513–525.

Ferry, J. M. (1991). Dehydration and decarbonation reactions as a record of fluid infiltration. In: Kerrick, D. M. (ed.) Contact Metamorphism. *Reviews in Mineralogy* **26**, 351–393.

Ferry, J. M. (2001). Calcite inclusions in forsterite. *American Mineralogist* **86**, 773–779.

Ferry, J. M. & Gerdes, M. L. (1998). Chemically reactive fluid flow during metamorphism. *Annual Review of Earth and Planetary Sciences* **26**, 255–287.

Ferry, J. M. & Rumble, D. (1997). Formation and destruction of periclase by fluid flow in two contact aureoles. *Contributions to Mineralogy and Petrology* **128**, 313–334.

Frantz, J. & Weisbrod, A. (1974). Infiltration metasomatism in the system K_2O–Al_2O_3–SiO_2–H_2O–HCl. In: Hofmann, A. W., Giletti, B. J., Yoder, H. S., Jr, & Yund, R. A. (eds) *Geochemical Transport and Kinetics*. Washington, DC: Carnegie Institution of Washington, pp. 261–271.

Frantz, J. D. & Mao, H. K. (1976). Bimetasomatism resulting from intergranular diffusion. 1. Theoretical model for monomineralic reaction zone sequences. *American Journal of Science* **276**, 817–840.

Galwey, A. K. & Jones, K. A. (1963). An attempt to determine mechanism of a natural mineral-forming reaction from examination of products. *Journal of the Chemical Society*, 5681–5686.

Galwey, A. K. & Jones, K. A. (1966). Crystal Size Frequency Distribution of Garnets in Some Analysed Metamorphic Rocks from Mallaig Inverness Scotland. *Geological Magazine* **103**, 143-&.

Gerdes, M. L., Baumgartner, L. P., Person, M., Rumble, D. & , III (1995). One- and two-dimensional models of fluid flow and stable isotope exchange at an outcrop in the Adamello contact aureole, southern Alps, Italy. *American Mineralogist* **80**, 1004–1019.

Gerdes, M. L., Baumgartner, L. P. & Valley, J. W. (1999). Stable isotopic evidence for limited fluid flow through dolomitic marble in the Adamello contact aureole, Cima Uzza, Italy. *Journal of Petrology* **40**, 853–872.

Grobéty, B. (1986). *Geologie und Petrographie des Adamellomassivs XII: Cima d'Uzza, Val Daone, Italien*. Zürich: ETHZ.

Hirsch, D. M. & Carlson, W. D. (2006). Variations in rates of nucleation and growth of biotite porphyroblasts. *Journal of Metamorphic Geology* **24**, 763–777.

Hirsch, D. M., Ketcham, R. A. & Carlson, W. D. (2003). An evaluation of spatial correlation functions in textural analysis of metamorphic rocks. *American Mineralogist* **88**, 1173.

Holland, T. & Powell, R. (2001). Calculation of phase relations involving haplogranitic melts using an internally consistent thermodynamic dataset. *Journal of Petrology* **42**, 673–683.

Korzhinskii, D. S. (1965). The theory of systems with perfectly mobile components and processes of mineral formation. *American Journal of Science*. New Haven, CT, United States, United States: Kline Geology Laboratory, Yale University, pp. 193–205.

Kretz, R. (1966). Grain-size distribution for certain metamorphic minerals in relation to nucleation and growth. *Journal of Geology* **74**, 147–173.

Kretz, R. (1969). On the spatial distribution of crystals in rocks. *Lithos* **2**, 39–66.

Kretz, R. (1993). A garnet population in Yellowknife schist, Canada. *Journal of Metamorphic Geology* **11**, 101–120.

Lasaga, A. C. (1998). *Kinetic Theory in Earth Sciences*. Princeton, NJ: Princeton University Press.

Lasaga, A. C. & Rye, D. M. (1993). Fluid flow and chemical reaction kinetics in metamorphic systems. *American Journal of Science* **293**, 361–404.

Lewis, S., Holness, M. & Graham, C. (1998). Ion microprobe study of marble from Naxos, Greece: Grain-scale fluid pathways and stable isotope equilibration during metamorphism. *Geology* **26**, 935–938.

Lichtner, P. C. (1996). Continuum formulation of multicomponent–multiphase reactive transport. *Reactive Transport in Porous Media* **34**, 1–81.

Marsh, B. D. (1998). On the interpretation of crystal size distributions in magmatic systems. *Journal of Petrology* **39**, 553–599.

Matile, L. & Widmer, T. (1993). Contact-metamorphism of siliceous dolomites, marls and pelites in the SE contact aureole of the Bruffione intrusion (SE Adamello, N Italy). *Schweizerische Mineralogische und Petrographische Mitteilungen* **73**, 53–67.

McRae, T. A. (1982). Contact-metamorphism of the Adamello Complex. *Journal of the Geological Society, London* **139**, 367–367.

Moazzen, M. & Modjarrad, M. (2005). Contact metamorphism and crystal size distribution studies in the Shivar aureole, NW Iran. *Geological Journal* **40**, 499–517.

Müller, T., Baumgartner, L. P., Foster, C. T., Jr, & Vennemann, T. W. (2004). Metastable prograde mineral reactions in contact aureoles. *Geology* **32**, 821–824.

Müller, T., Baumgartner, L. P., Foster, C. T., Jr & Bowman, J. R. (2008). Forward modeling of the effects of mixed volatile reaction, volume diffusion and formation of submicroscopic exsolution lamellae on calcite–dolomite thermometry. *American Mineralogist* **93**, 1245–1259.

Nabelek, P. I., Labotka, T. C. & Russnabelek, C. (1992). Stable isotope evidence for the role of diffusion, infiltration, and local-structure on contact-metamorphism of calc-silicate rocks at Notch Peak, Utah. *Journal of Petrology* **33**, 557–583.

Pennacchioni, G., Di Toro, G., Brack, P., Menegon, L. & Villa, I. M. (2006). Brittle–ductile–brittle deformation during cooling of tonalite (Adamello, Southern Italian Alps). *Tectonophysics* **427**, 171–197.

Roselle, G. T., Baumgartner, L. P. & Chapman, J. A. (1997). Nucleation-dominated crystallization of forsterite in the Ubehebe Peak contact aureole, California. *Geology* **25**, 823–826.

Roselle, G. T., Baumgartner, L. P. & Valley, J. W. (1999). Stable isotope evidence of heterogeneous fluid infiltration at the Ubehebe Peak contact aureole, Death Valley National Park, California. *American Journal of Science* **299**, 93–138.

Rubie, D. C. & Thompson, A. B. (1985). Kinetics of metamorphic reactions at elevated temperatures and pressures: an appraisal of available experimental data. In: Thompson, A. B. & Rubie, D. C. (eds) *Metamorphic Reactions: Kinetics, Textures, and Deformation*. New York: Springer, pp. 26–79.

Rumble, D. (1982). Stable isotope fractionation during devolatization reactions. In: Ferry, J. M. (ed.) *Characterization of Metamorphism through Mineral Equilibria. Mineralogical Society of America, Reviews in Mineralogy* **10**, 327–353.

Skora, S., Baumgartner, L. P., Mahlen, N. J., Johnson, C. M., Pilet, S. & Hellebrand, E. (2006). Diffusion-limited REE uptake by eclogite garnets and its consequences for Lu–Hf and Sm–Nd geochronology. *Contributions to Mineralogy and Petrology* **152**, 703–720.

Spear, F. S. (1993). *Metamorphic Phase Equilibria and Pressure–Temperature–Time Paths. Mineralogical Society of America Monograph*.

Spoetl, C. & Vennemann, T. W. (2003). Continuous-flow isotope ratio mass spectrometric analysis of carbonate minerals. *Rapid Communications in Mass Spectrometry* **17**, 1004–1006.

von Blanckenburg, F., Kagami, H., Deutsch, A., Oberli, F., Meier, M., Wiedenbeck, M., Barth, S. & Fischer, H. (1998). The origin of Alpine plutons along the Periadriatic Lineament. *Schweizerische Mineralogische und Petrographische Mitteilungen* **78**, 55–66.

Watson, E. B. (1996). Surface enrichment and trace-element uptake during crystal growth. *Geochimica et Cosmochimica Acta* **60**, 5013–5020.

Watson, E. B. & Liang, Y. (1995). A simple model for sector zoning in slowly grown crystals: Implications for growth rate and lattice diffusion, with emphasis on accessory minerals in crustal rocks. *American Mineralogist* **80**, 1179–1187.

Wersin, P. (1985). *Geologische Karte ueber das Gebiet von La Uzza und Monte*. Zürich: ETHZ, Mineralogisches Institut.

Yardley, B. W. D. & Lloyd, G. E. (1995). Why metasomatic fronts are really metasomatic sides. *Geology* **23**, 53–56.